Analyst

Accepted Manuscript

This article can be cited before page numbers have been issued, to do this please use: Y. Chen, W. Zhang, K. Huang, M. Zheng and Y. Mao, *Analyst*, 2017, DOI: 10.1039/C7AN01244F.

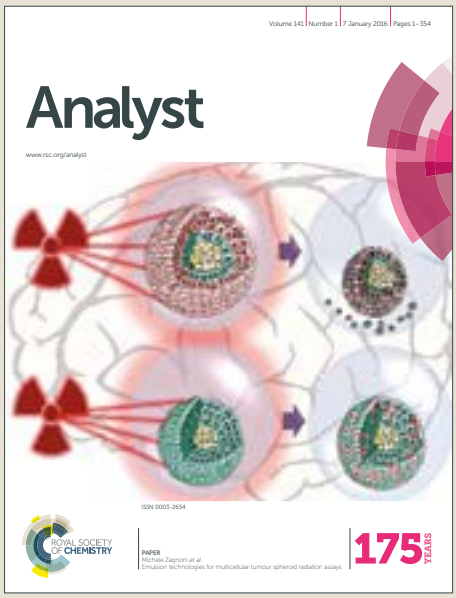

ROYAL SOCIETY OF CHEMISTRY

rsc.li/analyst

View Article Online
DOI: 10.1039/C7AN01244F

An electrochemical microRNA sensing platform based on tungsten diselenide nanosheets and competitive RNA-RNA hybridization

Ying-Xu Chen[a,b], Wen-Jing Zhang[a,b], Ke-Jing Huang[a,b*],Mingbo Zheng,[c] Ya-Cen Mao[a,b]

[a] *College of Chemistry and Chemical Engineering, Xinyang Normal University, Xinyang 464000, China*

[b] *Institute for Conservation and Utilization of Agro-bioresources in Dabie Mountains, Xinyang Normal University, Xinyang 464000, China*

[c] *School of Chemistry and Chemical Engineering, Yangzhou University, Yangzhou, 225002, Jiangsu, China.*

[*]Corresponding author. Tel.: +86-376-6390611

E-mail address: kejinghuang@163.com (K.J. Huang)

View Article Online
DOI: 10.1039/C7AN01244F

Abstract: In this work, we report an ultrasensitive electrochemical biosensor for microRNA-21 (miRNA-21) detection by using a competitive RNA-RNA hybridization configuration. A biotinylated miRNA of selfsame sequence with the target miRNA is mixed with the samples, and allowed competition with the target miRNA for a thiolated RNA probe immobilized onto tungsten diselenide (WSe_2) nanosheets modified electrode. Whereafter, the current response is obtained by forming the hybridized biotinylated miRNA with streptavidin-horseradish peroxidase (HRP) conjugates to catalyze H_2O_2+hydroquinone (HQ) system. Benefiting from high specific surface area of WSe_2 nanosheets, competitive hybridization configuration and signal amplification of H_2O_2+HQ detection system, the proposed assay exhibits a wide linear range of 0.0001-100 pM towards target miRNA with a detection limit of 0.06 fM (S/N=3), and shows excellent distinction ability for base-mismatched miRNA sequences. Therefore, the designed platform has promising prospects for detection of miRNA in biomedical research and early clinical diagnosis.

View Article Online
DOI: 10.1039/C7AN01244F

1. Introduction

MicroRNAs (miRNAs) belong to a class of small non-coding RNA molecules that play critical functions in many biological processes,[1] such as developmental regulation, proliferation, differentiation, cardiogenesis and epigenetic inheritance.[2-4] Currently, accumulative evidences have identified that abnormal expression of miRNA is highly correlated to the cancer initiation, oncogenesis and tumor response to treatments.[5-7] Moreover, miRNAs can be regarded as clinically important biomarkers for early cancer diagnostic, drug discovery targets and prognostic processes due to the presence of miRNAs in serum.[8,9] For instance, miRNA-21 plays an important role in a plethora of biological functions and diseases including development, cancer, cardiovascular diseases and inflammation.[10] Recently, additional roles of miRNA-21 in cardiovascular, pulmonary diseases, cardiac and pulmonary fibrosis as well as myocardial infarction have been described.[11] Due to the significant functions of miRNA-21 in human healthy, it has become an attractive target for genetic and pharmacological modulation in various disease conditions. As a consequence, it's imperative to develop more simple and sensitive method for miRNA detection in clinical cases.

Due to some intrinsic properties of miRNA, such as short size, high sequence similarity, low-level concentration in samples, conventional methods for miRNAs detection including Northern blotting, sequencing, quantitative polymerase chain reaction (qPCR) and microarray show some drawbacks in practical applications, such as poor sensitivity, time-consuming, expensive and complicated instruments.[12-14]

View Article Online
DOI: 10.1039/C7AN01244F

Recently, electrochemical biosensors get wide attention because of its great advantages of low-cost, simplicity of construction, high sensitivity and selectivity. However, for high sensitive detection of miRNA, most electrochemical biosensors require a variety of signal amplification strategies, such as hybridization chain reaction (HCR),[15,16] catalyzed hairpin assembly (CHA),[17,18] rolling circle amplification[19] and duplex-specific nuclease.[20,21] Definitely, the amplification strategies can significantly enhance the sensitivity of biosensor, but these strategies have shown some defects, such as expensive reagents and stringent external environmental requirement. In order to solve these difficulties, competitive binding strategies have been developed, which are widely used to detect small molecules in environmental and food safety monitoring.[22] For example, Yao et al. reported an exchange-induced remnant magnetization technique for let-7a assay with single-base specificity based on sequence-specific exchange reactions.[23] Wang et al. fabricated a fluorescence quenching of gold nanoparticles with a competitive hybridization to detect miRNA.[24]

For improving detection sensitivity, specific nanomaterials are usually used in the development of miRNA biosensor.[25-28] Recently, two-dimensional (2D) transition metal dichalcogenides have attracted considerable attention in batteries, biosensing, supercapacitor and electrocatalysis due to their large specific surface areas, good catalytic properties and chemical stability.[29-36] As a key member of 2D layered materials, WSe_2, with a structure composed of three stacked atom layers (Se-W-Se) bonded together by Van der Waals forces,[37] has been explored to be a promising

View Article Online
DOI: 10.1039/C7AN01244F

material for various fields, such as hydrogen evolution,[38-40] dye-sensitized solar cells,[41] photocatalytic[42] and field-effect transistors.[43] Interestingly, compared to the intensive research on MoS_2 and WS_2, the report of WSe_2 in electrochemical biosensing is lesser.[44,45] It has been reported WSe_2 has higher intrinsic electrical conductivity than WS_2 due to the more metallic nature of Se. And the unsaturated Se-edges in WS_2 are found to be electro-catalytically active and beneficial for the electrochemical sensing.

Herein, we report the development of a highly sensitive electrochemical platform for the detection of miRNA-21 using a competitive RNA-RNA hybridization configuration. Briefly, the target miRNAs compete with the biotinylated miRNAs for the hybridization of thiolated complementary capture probes which are assembled onto WSe_2 nanosheets modified electrode. The electrochemical response is carried out by forming the hybridized biotin-miRNA with streptavidin-horseradish peroxidase (HRP) conjugates to catalyze H_2O_2+hydroquinone (HQ) system. As a two-dimensional layered nanostructure, the as-prepared WSe_2 displayed a large effective surface area. This allowed more AuNPs loading on its surface to act as an excellent sensing substrate, which therefore can immobilize more biomolecules (capture DNA) to the electrode and in turn lead to a low detection limit. Under optimal experimental conditions, the proposed biosensor exhibited a sub-femtomolar detection limit for the target miRNA-21 with a wide linear range and good selectivity.

2. Experimental

View Article Online
DOI: 10.1039/C7AN01244F

2.1. Reagents and materials

Se powder, sodium borohydride ($NaBH_4$), $Na_2WoO_4 \cdot 2H_2O$, N, N-dimethylformamide (DMF), H_2O_2 and HQ were obtained from Aladdin Chemicals Co. Ltd. (Shanghai, China). 6-mercaptohexanol (MCH) and streptavidin-HRP were purchased from Sigma-Aldrich (Shanghai, China). The oligonucleotide was synthesized in Sangon Biotech Co. Ltd. (Shanghai, China):

MiRNA-21: 5'-UAGCUUAUCAGACUGAUGUUGA-3'

Bio-RNA: 5'-UAGCUUAUCAGACUGAUGUUGA-biotin-3'

SH-RNA: 5'-UCAACAUCAGUCUGAUAAGCUA-$(CH_2)_6$-SH-3'

Single-base mismatch: 5'-UAGCUUAUCGGACUGAUGUUGA-3'

Three-base mismatch: 5'-UUGCUUAUCGGACUGAUCUUGA-3'

Non-complementary: 5'-GUAAGGCAUCUGACCGAAGGCA-3'

The miRNAs stock solutions were prepared daily with diethylpyrocarbonate-treated water in an RNase-free environment.

2.2. Apparatus

Electrochemical measurements were tested on a RST5200F electrochemical workstation (Zhengzhou Shi Rui Si Instrument, Zhengzhou, China). The products morphologies were observed by using a JSM-6510 scanning electron microscopy (SEM, JEOL, Tokyo, Japan) at 20 V-30 kV and a JEM 2100F transmission electron microscopy (TEM, JEOL, Tokyo, Japan). A model D/max-rA diffractometer (Rigaku, Tokyo, Japan) was used to record X-ray diffraction (XRD) data. N_2

View Article Online
DOI: 10.1039/C7AN01244F

adsorption/desorption isotherms were carried out on an ASAP2020 surface area and porosity analyzer (Micrometrics Instrument Co., Shanghai, China). Raman spectra was recorded on a Raman system model 1000 spectrometer (Renishaw, Gloucestershire, UK). The chemical composition of the as-prepared product was examined by a K-ALPHA 0.5EV X-ray Photoelectron Spectrometer (XPS, Thermo Fisher Scientific, Massachusetts, USA).

2.3. Synthesis of WSe_2 nanosheets

WSe_2 nanosheets were synthesized by one-pot solvothermal method. Typically, 0.64 g of Se powder, 0.20 g of NaBH4 and 1.32 g of $Na_2WO_4 \cdot 2H_2O$ were dispersed in 60 mL DMF. The mixture was continually stirred for 2 h. Subsequently, the mixture was transferred into a Teflon-lined stainless steel autoclave and kept at 200 °C for 72 h. The black precipitate was collected by centrifugation, washed with DI water and ethanol for several times, dried at 60 °C for 12 h.

2.4. Preparation of aptasensor

Firstly, the glass carbon electrode (GCE) was pretreated by alumina slurry. Then, 6.0 μL of WSe_2 suspension (1 mg/mL) was applied on the pretreated GCE surface and dried in air to obtain WSe_2/GCE. To immobilize thiolated RNA (SH-RNA), the AuNPs was electrodeposited on electrode in 0.1% $HAuCl_4$ solution at −0.2 V for 20 s. Whereafter, 6 μL SH-RNA (0.5 μM) was cast onto the AuNPs/WSe_2/GCE and incubated for 12 h. After rinsed with water, 4 μL of 1 mM MCH was dropped on the

View Article Online
DOI: 10.1039/C7AN01244F

SH-RNA/AuNPs/WSe_2/GCE and reacted for 30 min to eliminate nonspecific adsorption. Again, 8 μL mixture of different concentration of miRNA-21 and 1 μM Bio-RNA were applied on electrode and incubated at 37 ℃ for 80 min. Finally, 8 μL of streptavidin-HRP (0.5 μM) was applied upon electrode and kept at room temperature for 40 min.

For targets sensing, cyclic voltammetry (CV) was carried out in 0.1 M phosphate buffer saline (PBS, pH 7.0) containing 10 mmol L^{-1} $[Fe(CN)_6]^{3-/4-}$ and 0.1 mol L^{-1} KCl solution with a scan rate of 100 mVs^{-1}. Electrochemical impedance spectroscopy (EIS) measurements were performed in 0.1 M PBS (pH 7.0) containing 5.0 mmol L^{-1} $[Fe(CN)_6]^{3-/4-}$ and 0.1 mol L^{-1} KCl solution, with the voltage amplitude of 5 mV and voltage frequencies from 100 kHz to 0.1 Hz at the applied potential of 0.2 V. Differential pulse voltammetry (DPV) measurements were conducted in 0.1 M PBS (pH 7.0) containing 1.8 mM H_2O_2 and 2 mM HQ using a pulse amplitude of 50 mV, pulse width of 50 ms, pulse period of 0.2 s. The direction of the scan was from negative to positive and the potential range was from -0.4 to 0.2V.

2.5. Detection of miRNA-21 in human serum

Serum samples of patients were obtained from the affiliated hospital of Xinyang Normal University. Firstly, 0.1 mL serum was added in 1.0 mL PBS. Then the serum sample and detected by the obtained calibration curve of the developed biosensor. All these experiments were performed in compliance with the relevant laws and institutional guidelines and the ethics committee that approved these experiments was

View Article Online
DOI: 10.1039/C7AN01244F

the Institutional Review Board of the affiliated hospital of Xinyang Normal University. Informed consent was also given by every participant.

3. Results and discussion

3.1. Design principle of biosensor

Fabrication principle of as-prepared miRNA biosensor is illustrated in Scheme 1. Firstly, SH-RNA is fixed on AuNPs/WSe_2 modified electrode. Then, MCH is dropped on the electrode surface to block the free sites. Subsequently, the mixture of different concentration of miRNA-21 and Bio-RNA are applied on electrode. In this step, the largest DPV response is carried out by using H_2O_2 as enzyme substrate and HQ as redox mediator in the absence of traget miRNA. However, an obvious decrease DPV response is observed in the presence of the target miRNA due to the target miRNA competing with the biotinylated miRNA for hybridization with the thiolated RNA and results in a small quantity of biotinylated miRNA on the electrode to attach streptavidin-HRP. The oxidation current of detection system decreases prominently with the increase of miRNA-21 concentration. Therefore, the current variation ΔI ($\Delta I=I-I_0$, where I and I_0 represent the peak currents in the presence and absence of miRNAs, respectively) is used to evaluate the analytical merits for detection of miRNA.

View Article Online
DOI: 10.1039/C7AN01244F

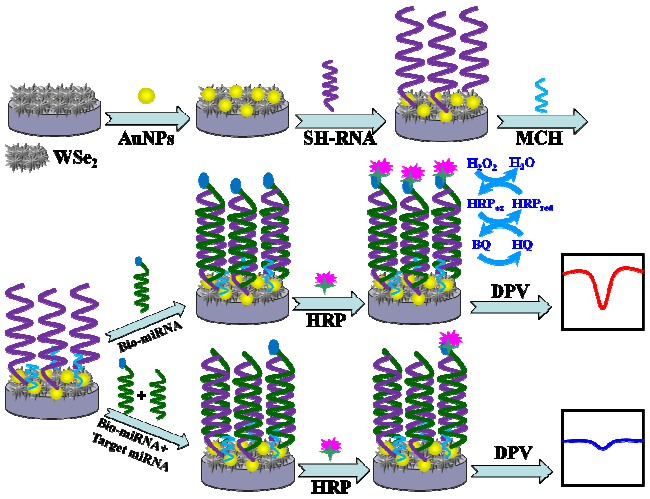

Scheme 1. Schematic illustration of the biosensor for detection of miRNA by using competitive hybridization configuration.

3.2. Materials characterization

XRD and Raman spectroscopy were used to study the WSe_2 sample. As shown in Fig. 1A, in the XRD patterns of the WSe_2, all major diffraction peaks match well with the typical hexagonal structure of WSe_2 (JCPDS card No. 38-1388). The diffraction peaks at 13.34°, 34.64°, 41.36°, 46.43°, 55.92° and 66.13° are corresponding to the (002), (100), (103), (105), (110) and (108) crystal planes of WSe_2, respectively. Moreover, no miscellaneous diffraction peaks are observed, indicating that WSe_2 is quite pure. To further investigate the nanostructure of WSe_2, the Raman spectrum of WSe_2 is shown in Fig. 1B. A characteristic peak at 249 cm^{-1} is corresponding to E^1_{2g} Raman mode of WSe_2, and is consistent with the W-Se band of hexagonal WSe_2. Therefore, the XRD patterns and Raman spectra results show the successful synthesis of WSe_2.

Moreover, the chemical composition of the WSe_2 sample was verified by XPS.

View Article Online
DOI: 10.1039/C7AN01244F

The XPS spectrum indicates that the WSe_2 is composed of W, Se, and O (Fig. 1 C). In Fig. 1 D, the peaks at 54.2 eV and 55 eV are consistent with the Se $3d_{5/2}$ and Se $3d_{3/2}$, respectively.[36] As shown in Fig. 1 E, two distinct peaks at 35 and 32.7 eV are assigned to W $4f_{5/2}$ and W $4f_{7/2}$, respectively.[36] A peak at 37.1 eV is attributed to the W-O bond due to the +6 oxidation state of surface W atom.[44] In addition, the detailed compositional analysis showed that the atomic ratio of Se to W is 2.01, approaching the theoretical atomic ratio of WSe_2.

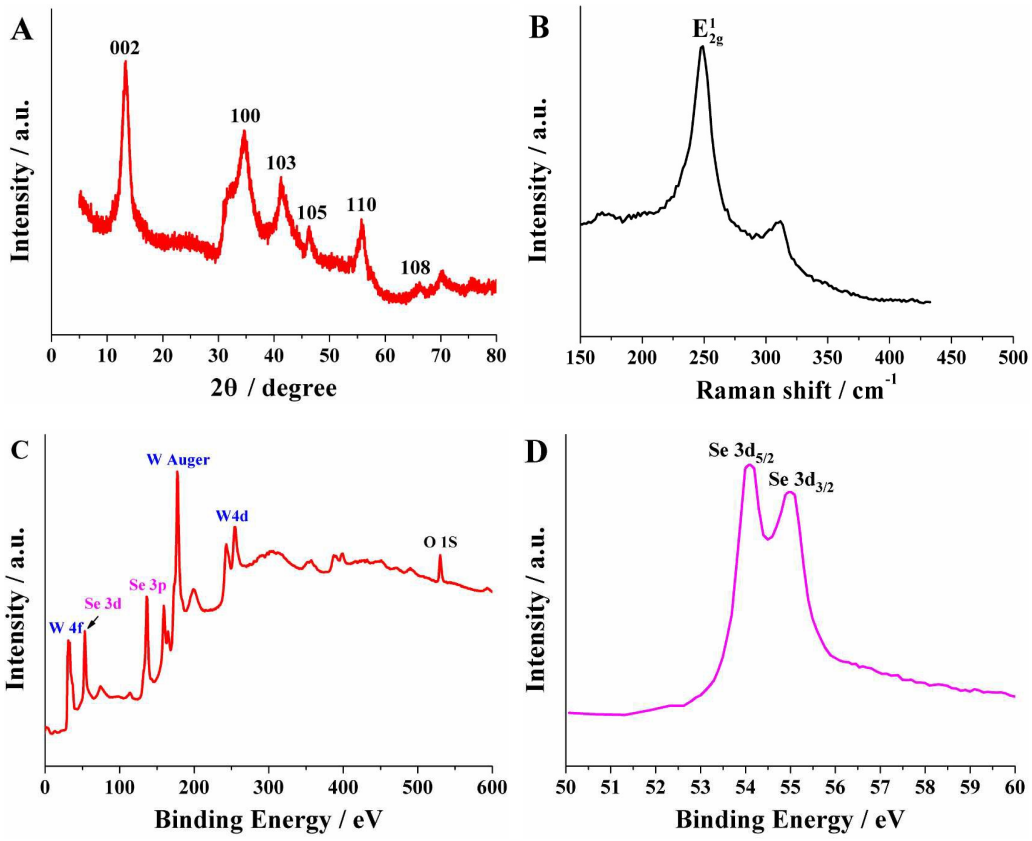

View Article Online
DOI: 10.1039/C7AN01244F

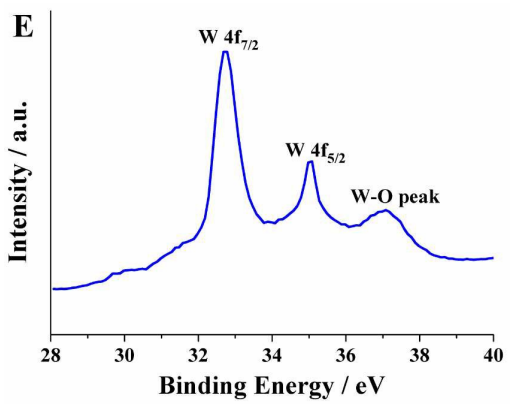

Fig. 1. The XRD pattern (A), Raman spectra (B) and XPS spectrum (C) of WSe_2; high-resolution XPS spectra of Se 3d (D) and (E) W 4f of WSe_2.

Morphologies of the as-obtained samples were characterized with SEM and TEM. SEM images of WSe_2 are shown in Fig. 2A and B. It can expressly observe that the WSe_2 possesses an ultrathin sheet nanostructure. WSe_2 nanosheets interwoven with each other, providing rich active edges for sensing platform. As displayed in Fig. 2C, the TEM images exhibit again the ultra-thin nanosheets of WSe_2. HRTEM was also use to investigate the structure of WSe_2 nanosheets. As shown in Fig. 2D, the lattice spacing of 0.68 nm and 0.285 nm are observed corresponding to the (002) and (100) plane of the 2H-WSe_2,[45] respectively, which consists with the XRD result.

The elemental composition of the WSe_2 is examined by EDX analysis (Fig. 2E). The spectrum shows that the samples are composed of W and Se elements. As shown in the inset, the atomic ratio of W to Se is calculated as 1:2.05, indicating the successful preparation of WSe_2 nanosheets. The mass fraction of W and Se are 51.78% and 48.22%, respectively.

View Article Online
DOI: 10.1039/C7AN01244F

Brunauer–Emmett–Teller (BET) specific surface area and porous structure of WSe_2 nanosheets were measured by nitrogen adsorption–desorption analysis (Fig. 2 F). The results show the BET specific surface area of the WSe_2 nanosheets is 26.4 $m^2 g^{-1}$, which is higher than that of previous report (19.6 m^2/g).[38] The pore size distribution shown in the inset demonstrates the pore diameters of WSe_2 is about 3.5 nm. The considerably large surface area and porous structure of WSe_2 nanosheets can provide more active sites and large space for the deposition of AuNPs and the subsequent immobilization of SH-RNA, which are favorable to structure high-performance biosensor.

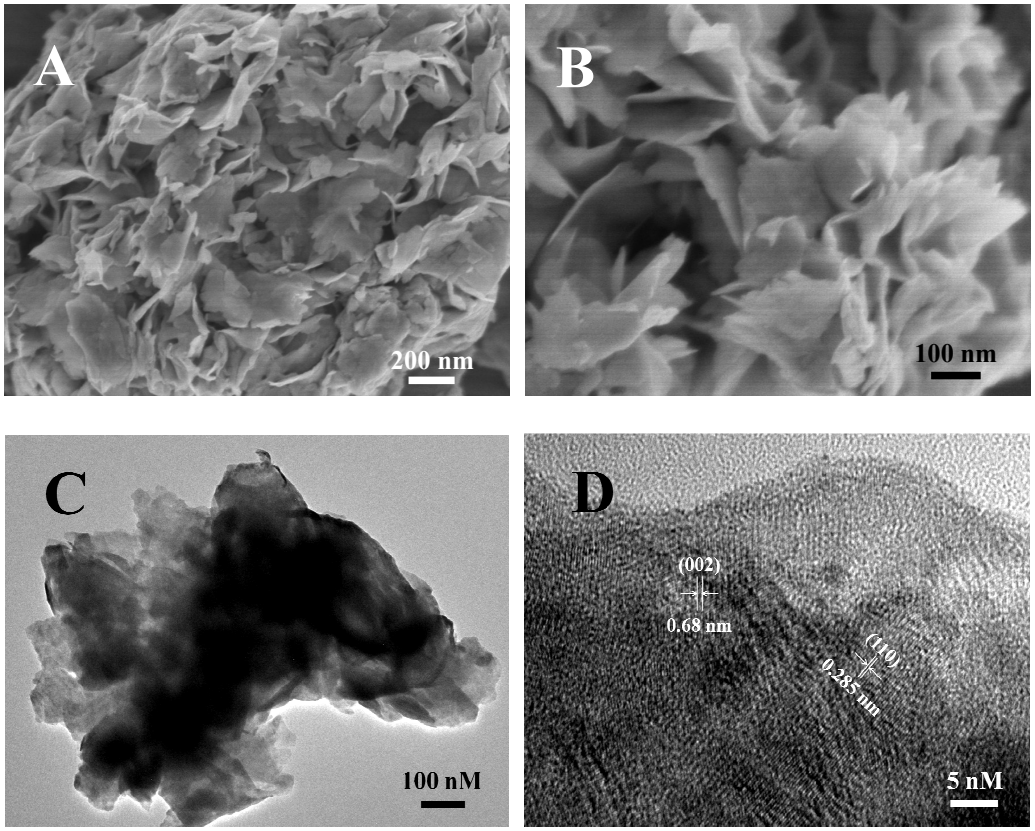

View Article Online
DOI: 10.1039/C7AN01244F

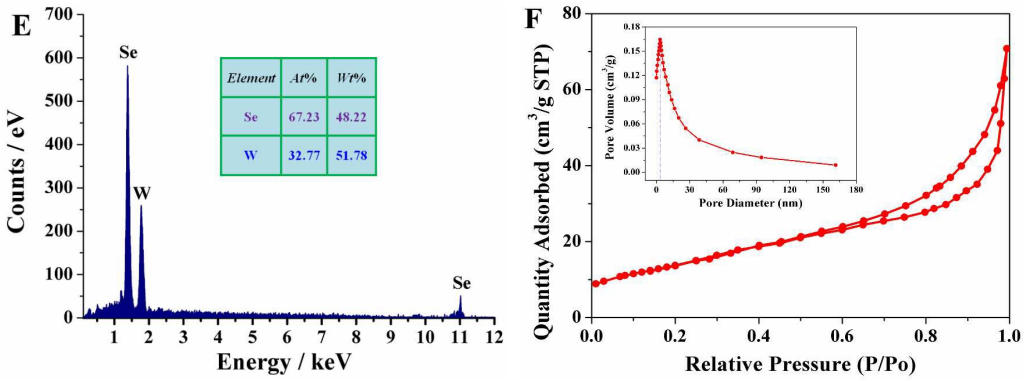

Fig. 2 The SEM images (A, B), TEM image (C), HETEM image (D), EDX spectra (E), and the BET (F) of WSe_2 nanosheets.

3.3. Electrochemical behaviors

CV was used to characterize different modified electrodes, as shown in Fig. 3A, WSe_2 sheets show the comparable redox peak current (curve b) to the GCE (curve a) due to its semiconductor characters. However, a greatly enhanced current response is distinctly observed (curve c) after AuNPs are further coated on the electrode, mainly owing to the large specific surface area of WSe_2 sheets can load abundant AuNPs which have high conductivity and can accelerate the electron transfer. Fig. 3B displays the decrease of electrochemical responses of different modified electrodes. When SH-RNA is further immobilized (curve d), the current response of electrode decreases due to miRNA strands make the electrode surface highly negatively charged and the electron transfer become difficult. The current response further decreases after MCH are coated on the electrode (curves e) because MCH insulates electrode surface leading to electron transfer turning into difficult. Likewise, when target RNA+bio-RNA are further applied on the electrode (curves f), the current

View Article Online
DOI: 10.1039/C7AN01244F

response is further decreased for the fact that more negatively charged SH-RNA/traget miRNA or SH-RNA/bio-miRNA duplex loaded on the electrode surface, which hinders the electron transfer. The current response obviously decreases (curve g) when streptavidin-HRP is subsequently modified on the electrodes because biological macromolecules insulate the electrodes surface. From these CV results, successful construction of the biosensor can be confirmed.

In order to prove the effect of WSe_2 nanosheets, the EIS of AuNPs/WSe_2/GCE and AuNPs/GCE was measured (Fig. 3C). Diameter of the semicircle in the resulting pattern can index the interfacial electron transfer resistance (R_{et}) of the electrode. Distinctly, the R_{et} value of AuNPs/WSe_2/GCE (curve a) is smaller than AuNPs/GCE (curve b), indicating that WSe_2 nanosheets make contribution to immobilized more AuNPs to enhance the electron conductivity.

The effective surface areas (A) of biosensor and bare GCE were evaluated by chronocoulumetry, and calculated based on following equation:

$$Q = 2nFAcD^{1/2}t^{1/2}/\pi^{1/2} + Q_{dl} + Q_{ads} \quad (1)$$

where n, F, c, Q_{dl} and Q_{ads} (C) are the number of electron transferred, Faraday constant, concentration of substrate, diffusion coefficient, double layer charge, adsorption charge, respectively. The others have their usual significances. From Fig. 3D, A is calculated to be 0.017 cm^2 and 0.096 cm^2 for bare GCE and AuNPs/WSe_2/GCE, respectively, confirming AuNPs/WSe_2 greatly improve the effective surface area of electrode to amplify the electrical signal.

View Article Online
DOI: 10.1039/C7AN01244F

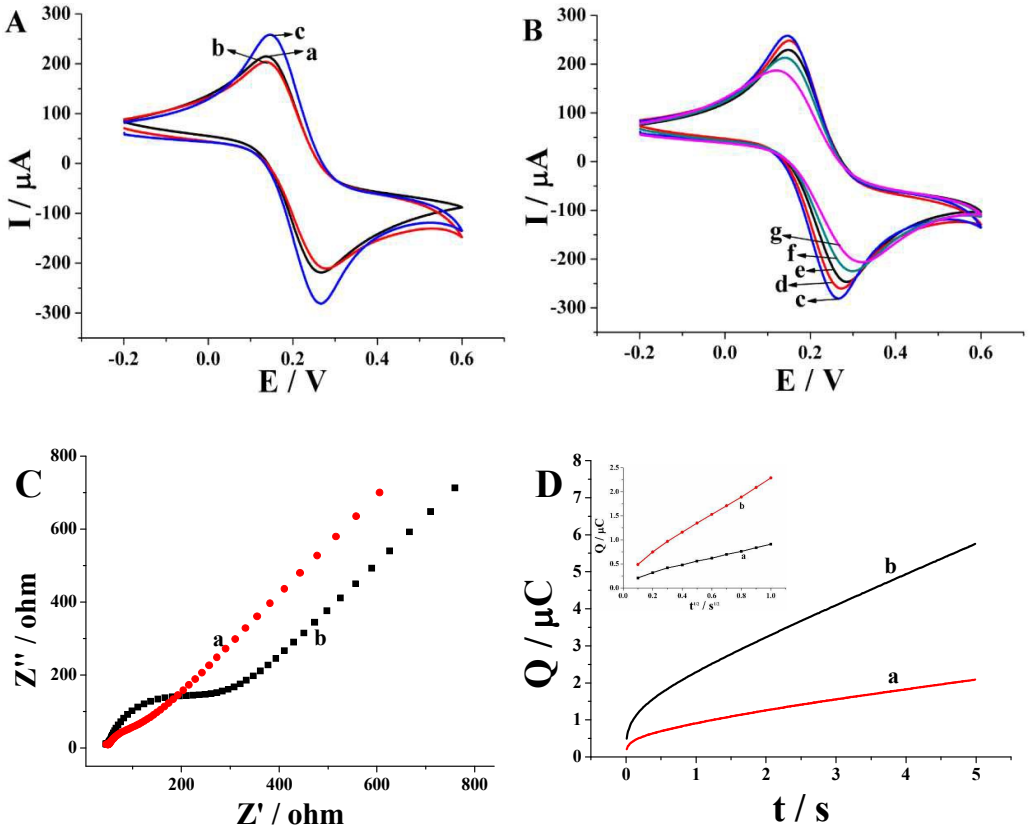

Fig. 3. CVs (A, B) of GCE (a), WSe_2/GCE (b), AuNPs/WSe_2/GCE (c), SH-RNA/AuNPs/WSe_2/GCE (d), MCH/SH-RNA/AuNPs/WSe_2/GCE (e), target miRNA+Bio-miRNA/MCH/SH-RNA/AuNPs/WSe_2/GCE (f), streptavidin-HRP/target miRNA+Bio-miRNA/MCH/SH-RNA/AuNPs/WSe_2/GCE (g); (C) EIS of AuNPs/WSe_2/GCE (a) and AuNPs/GCE (b); (D) plot of Q-t curves of GCE (a) and AuNPs/WSe_2/GCE (b). Inset: Q-$t^{1/2}$ curves of GCE (a) and AuNPs/WSe_2/GCE (b).

3.4. Optimization of experimental conditions

Several experimental conditions were optimized in order to acquire good performance of the developed miRNA biosensor. The effect of deposition time of AuNPs on electrochemical signal is studied from 10 to 60 s (Fig. 4A). CV signal

View Article Online
DOI: 10.1039/C7AN01244F

increases greatly from 10 to 20 s, and then almost stays stable after 20 s. So, deposition time of 20 s is used.

The effect of concentration of SH-RNA was evaluated. The biggest current response is obtained when the concentration of SH-RNA is 0.5 μM (Fig. S1A). The effect of incubation time between target RNA+bio-RNA and SH-RNA is also studied. The current response increases promptly with the incubation time ranging from 20 to 80 min. It then nearly stays unchanged when exceeds 80 min. So, incubation time of 80 min is employed (Fig. 4B).

The effect of immobilization of streptavidin-HRP is studied. Fig. 4C shows peak currents increase from 20 to 120 min and then keep almost unchanged after 40 min. The result indicates the most streptavidin-HRPs have been immobilized on electrode surface at 40 min. So, 40 min is used. The amount of streptavidin-HRP is also optimized (Fig. S1B). The result indicates that the current signal reaches the highest when the amount of streptavidin-HRP is 0.5 μM. So, 0.5 μM of streptavidin-HRP is used.

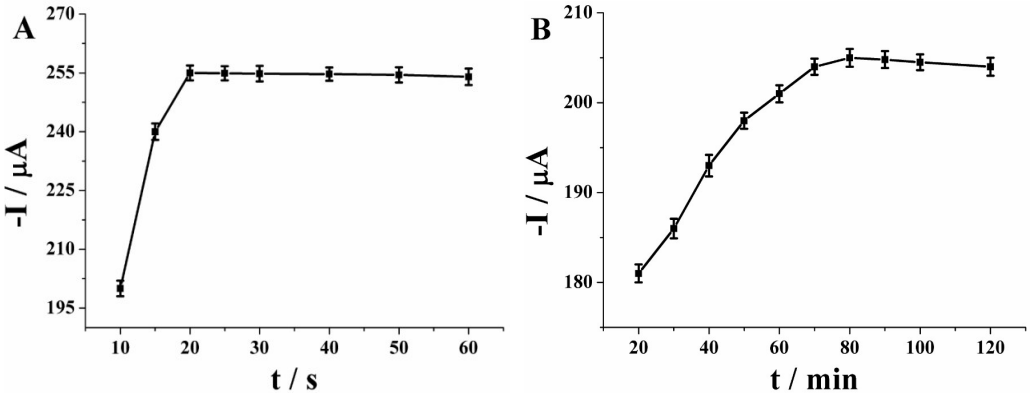

View Article Online
DOI: 10.1039/C7AN01244F

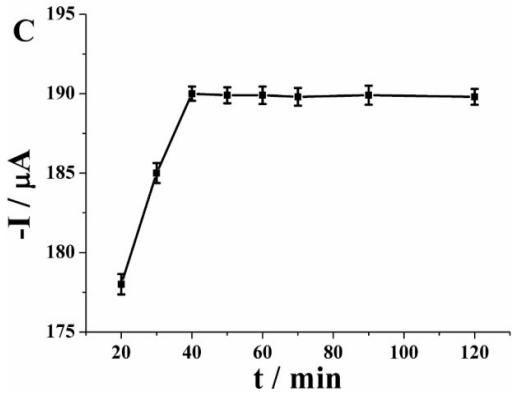

Fig. 4. Influence of deposition time of AuNPs (A), incubation time of target RNA +bio-RNA and SH-RNA (B), and immobilization time of streptavidin-HRP (C) on peak current.

3.5. Analytical performance of designed biosensor

Under optimum conditions, the proposed biosensor was applied to determine miRNA-21 by DPV. Fig. 5A shows peak currents increase with decreasing the concentration of miRNA-21. In our work, the current variation ΔI ($\Delta I=I-I_0$, where I and I_0 represent the peak currents in the presence and absence of miRNAs, respectively) is used to detect miRNA. As shown in the inset of Fig. 5A, DPV currents shows a good linear relation with the logarithm of miRNA-21 concentration ranging from 0.1 fM to 100 pM. The linear calibration equation is ΔI = 70.05 + 4.32log(c/M) with correlation coefficient R of 0.997 and detection limit of 0.06 fM (S/N=3). The analytical performances of different assays for miRNA detection are compared in Table 1. The proposed assay exhibits the lowest detection limit and the widest detection range which is attributed to the dual signal amplification of competitive hybridization configuration strategy and WSe_2 nanosheets.

View Article Online
DOI: 10.1039/C7AN01244F

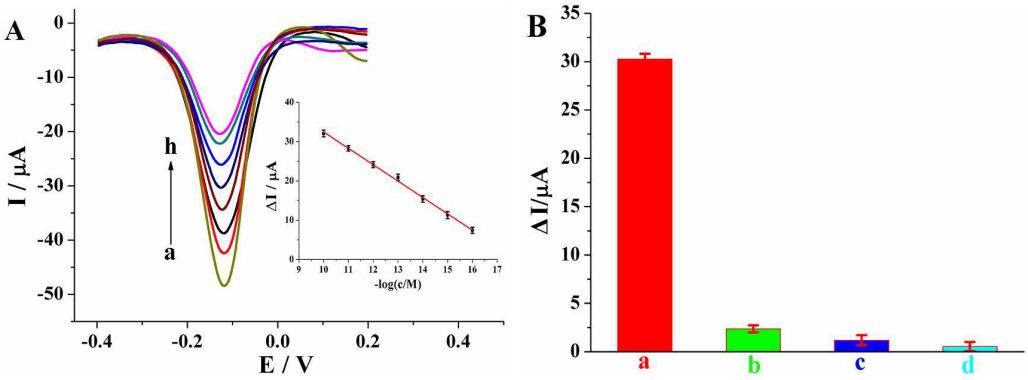

Fig. 5. (A) DPVs of various target miRNA concentrations (from a to h): 0, 1.0×10^{-16}, 1.0×10^{-15}, 1.0×10^{-14}, 1.0×10^{-13}, 1.0×10^{-12}, 1.0×10^{-11}, 1.0×10^{-10} M, respectively. Inset: calibration plots of the DPV currents variation ΔI versus the negatively logarithm of target miRNA concentrations. Error bars show the standard deviations of measurements taken from three independent experiments; (C) the selectivity of the sensor in the presence of different target miRNA sequences: miRNA (a), single-based mismatch sequence (b), three-based mismatch sequence (c) and non-complementary sequence (d).

View Article Online
DOI: 10.1039/C7AN01244F

Table 1. Comparison of different biosensors for miRNA determination.

Strategy	Method	Linear range	LOD	Ref.
Mismatched CHA	Electrochemistry	1 pM–25 nM	0.6 pM	8
HCR	Colorimetric	1 pM–100 pM	31.8 fM	13
AuNPs loaded DNA	Fluorescence	100 pM–300 nM	10 pM	48
Tetrahedral DNA for simultaneous detection	Electrochemistry	10 fM–1 nM	10 fM	49
Target-guide assembly of AuNPs	ECL	40 fM–1 pM	20 fM	50
Graphene oxide-AuNPs as carrier	SPR	0.1 pM–2 nM	0.1 fM	51
Toluidine blue as a redox indicator and AuNPs superlattice as support material	Electrochemistry	0.1fM–1nM	0.078fM	52
AuNPs-decorated MoS_2 nanosheet	Electrochemistry	10 fM to 1 nM	0.78 fM	53
Competitive RNA-RNA hybridization	Electrochemistry	0.0001–100 pM	0.06 fM	This work

3.6. Selectivity, reproducibility and stability

The selectivity of the proposed biosensor was validated by comparing DPV current variation with different miRNA sequences. As shown in Fig. 5B, the highest

View Article Online
DOI: 10.1039/C7AN01244F

ΔI is obtained with target miRNA-21. The ΔIs of non-complementary sequence and both mismatched sequence are low and negligible, indicating these sequences are incapable of competing with bio-RNA to hybridize with SH-RNA. Particularly, the higher ΔI of single-base mismatched sequence is only 7.7% of that of target miRNA. These results indicated good selectivity of the developed assay. Moreover, five equally prepared electrodes were used to detect miRNA-21 of 1.0 and 0.01 pM, and the relative standard deviations (RSD) were 4.3% and 2.1%, respectively, indicating proposed assay had good reproducibility. To further evaluate the stability of the biosensor, the as-prepared biosensor was kept under 4 °C for 15 days and 96.7% of the initial response to 1 pM miRNA-21 can still be remained, suggesting its good stability.

3.7. Real sample analysis

We further investigated the feasibility of this method to real samples by testing the miRNA-21 in three human serum samples from breast cancer patients. The same samples were also experiment by RT-PCR method. As shown in Table 2. The results obtained with the proposed assay are in good agreement with that by qRT-PCR, suggesting that the present assay is available for determining miRNA in real samples.

View Article Online
DOI: 10.1039/C7AN01244F

Table 2. Detection of miRNA-21 in human serum samples (n = 3).

Samples	qRT-PCR (fM)[a]	Proposed assay (fM)[a]
1	37.6±2.3	36.1±3.6
2	34.5±2.5	35.8±4.2
3	33.2±1.9	34.1±3.1

[a] Average of three determinations ± standard deviation.

4. Conclusion

In summary, a sensitive electrochemical biosensor for the detection of miRNA-21 is fabricated using a competitive configuration between the target miRNA and the biotinylated miRNA for the hybridization of a thiolated complementary RNA which is assembled on WSe_2 nanosheets modified electrode. The good performance of the biosensor is attributed to several aspects. Firstly, the large specific surface area of WSe_2 can load more AuNPs to enlarge exposure of edge sites for immobilizing biomolecules and accelerate the electron transfer rate. Secondly, competitive hybridization configuration strategy greatly increases the specificity and sensitivity of the assay. Thirdly, Hydrogen peroxide + Hydroquinone system is used to detect miRNA-21 for improving detection signal and results in an extraordinary low detection limit (0.068 fM). So, the proposed sensor has a high potential in clinical application.

View Article Online
DOI: 10.1039/C7AN01244F

Acknowledgments

This work was supported by the National Natural Science Foundation of China (21475115), Program for University Innovative Research Team of Henan (15IRTSTHN001), Henan Provincial Science and technology innovation team (C20150026), Nanhu Scholars Program of XYNU, Henan Science and Technology Cooperation Project (172106000064) and Graduate Scientific Research Innovation Fund of Xinyang Normal University (No. 2016KYJJ12).

References

1 L. He and G. J. Hannon, *Nat. Rev. Genet.*, 2004, **5**, 522.

2 Y. L. Wei, W. J. Zhou, X. Li, Y. Q. Chai, R. Yuan and Y. Xiang, *Biosens. Bioelectron.*, 2016, **77**, 416.

3 H. L. Shuai, K. J. Huang, Y. X. Chen, L. X. Fang and M. P. Jia, *Biosens. Bioelectron.*, 2017, **89**, 989.

4 H. L. Shuai, K. J. Huang, L. L. Xing and Y. X. Chen, *Biosens. Bioelectron.*, 2016, **86**, 337.

5 X. Gong, W. J. Zhou, Y. Q Chai, R. Yuan and Y. Xiang, *Chem. Commun.*, 2016, **52**, 2501.

6 T. T. Zhang, H. M. Zhao, G. F. Fan, Y. X. Li, L. Li and X. Quan, *Electrochim. Acta*, 2016, **190**, 1150.

7 H. L. Shuai, K. J. Huang, W. J. Zhang, X. Y. Cao and M. P. Jia, *Sens. Actuators B*, 2017, **243**, 403.

8 Y. Zhang, Y. R. Yan, W. H. Chen, W. Cheng, S. Q. Li, X. J. Ding, D. D. Li, H. Wang,

View Article Online
DOI: 10.1039/C7AN01244F

H. X. Ju and S. J. Ding, *Biosens. Bioelectron.*, 2015, **68**, 343.

9 P. Zhang, Z. Y. Li, H. J. Wang, Y. Zhuo, R. Yuan and Y. Q. Chai, *Nanoscale*, 2017, **9**, 2310.

10 V. Jazbutyte and T. Thum, *Curr. Drug Ttargets*, 2010, **11**, 926.

11 R. Kumarswamy, I. Volkmann and T. Thum, *RNA Biology*, 2011, **8**, 706.

12 K. Shi, B. T. Dou, J. M. Yang, R. Yuan and Y. Xiang, *Anal. Chim. Acta*, 2016, **916**, 1.

13 P. T. Nelson, D. A. Baldwin, L. M. Scearce, J. C. Oberholtzer, J. W. Tobias and Z. Mourelatos, *Nat. Methods*, 2004, **1**, 155.

14 X. Y. Wu, Y. Q. Chai, P. Zhang and R. Yuan. *ACS Appl. Mater. Interfaces*, 2015, **7**, 713.

15 N. Ying, T. F. Sun, Z. B. Chen, G. P. Song, B. Y. Qi, S. J. Bu, X. W. Sun, J. Y. Wan and Z. H. Li, *Anal. Biochem.*, 2017, **528**, 7.

16 R. M. Torrente-Rodríguez, S. Campuzano, V. R. V. Montiel, J. J. Montoy and J. M. Pingarrón, *Biosens. Bioelectron.*, 2016, **86**, 516.

17 X. M. Li, W. Cheng, D. D. Li, J. L. Wu, X. J. Ding, Q. Cheng and S. J. Ding, *Biosens. Bioelectron.*, 2016, **80**, 98.

18 W. Cai, S. B. Xie, Y. Tang, Y. Q Chai, R. Yuan and J. Zhang, *Talanta*, 2017, **163**, 65.

19 A. Y. Chen, S. Y. Ma, Y. Zhuo, Y. Q. Chai and R. Yuan, *Anal. Chem.*, 2016, **88**, 3203.

20 L. Liu, Y. P. Gao, H. P. Liu and N. Xia. *Sens. Actuators B*, 2015, **208**, 137.

View Article Online
DOI: 10.1039/C7AN01244F

21 K. Zhang, K. Wang, X. Zhu, F. Xu and M. H. Xie, *Biosens. Bioelectron.*, 2017, **87**, 358.

22 Y. Zhang, A. H. Gao, B. Liu, W. Sheng, C. Tan, M. Yuan and S. Wang, *J. Environ. Sci. Health B*, 2013, **48**, 1.

23 L. Yao, Y. Wang and S. Xu, *Chem. Commun.* 2013, **49,** 5183.

24 W. Wang, T. Kong, D. Zhang, J. A. Zhang and G. S. Cheng, *Anal. Chem.*, 2015, **87**, 10822.

25 J. Li, D. X. Li, R. Yuan and Y. Xiang, *ACS Appl. Mater. Interfaces*, 2017, **9**, 5717.

26 Y. Q. Yu, J. P. Wang, M. Zhao, L. R. Hong, Y. Q. Chai, R. Yuan and Y. Zhuo, *Biosens. Bioelectron.*, 2016, **77**, 442.

27 K. H. Li, W. Liu, Y. Ni, D. P. Li, D. M. Lin, Z. Q. Su and G. Wei, *J. Mater. Chem. B*, 2017, DOI: 10.1039/c7tb01073g.

28 H. Y. Liu, L. N. Zhang, M. Yan and J. H. Yu, *J. Mater. Chem. B*, 2017, DOI: 10.1039/c7tb00891k.

29 L. Liao , J. Zhu , X. J. Bian , L. N. Zhu , M. D. Scanlon, H. H. Girault and B. H. Liu, *Adv. Funct. Mater.*, 2013, **23**, 5326.

30 J. Jin, B. Kim, M. Kim, N. Park, S. Kang, S. M. Lee, H. J. Kim and S. U. Son, *Nanoscale*, 2015, **7**, 11280.

31 H. L. Shuai, K. J. Huang and Y. X. Chen. *J. Mater. Chem. B*, 2016, **4**, 1186.

32 K. J. Huang, Y. J. Liu, H. B. Wang, Y. Y. Wang and Y. M. Liu. *Biosens. Bioelectron.*, 2014, **55**, 195.

33 H. L. Shuai, X. Wu and K. J. Huang, *J. Mater. Chem. B,* 2017, **5**, 5362.

View Article Online
DOI: 10.1039/C7AN01244F

34 K. J. Huang, J. Z. Zhang and Y. Fan, *Mater. Lett.*, 2015, **152**, 244.

35 S. Yu, J. Kim, K. R. Yoon, J. W. Jung, J. Oh and D. Kim. *ACS Appl. Mater. Interfaces*, 2015, **7**, 28116.

36 B. Guo, K. Yu, H. Li, H. Song, Y. Zhang, X. Lei, H. Fu, Y. Tan and Z. Zhu. ACS *ACS Appl. Mater. Interfaces*, 2016, **8**, 5517.

37 X. Q. Wang, Y. F. Chen, F. Qi, B. J. Zheng, J. R. He, Q. Li, P. J. Li, W. L. Zhang and Y. R. Li. *Electrochem. Commun.*, 2016, **72**, 74.

38 M. L. Zou, J. F. Zhang, H. Zhu, M. L. Du, Q. F. Wang, M. Zhang and X. W. Zhang. *J. Mater. Chem. A*, 2015, **3**, 12149.

39 D. A. Henckel, O. Lenz and B. M. Cossairt, *ACS Catal.*, 2017, **7**, 2815.

40 X. Q. Wang, Y. F. Chen, B. J. Zheng, F. Qi, J. R. He, Q. Li, P. J. Li and W. L. Zhang, *J. Alloy. Compd.*, 2017, **691**, 698.

41 S. Hussain, S. A. Patil, D. Vikraman, A. A. Arbab, S. H. Jeong, H. S. Kim and J. Jung, *Appl. Surf. Sci.*, 2017, **406**, 84.

42 X. Q. Wang, Y. F. Chen, B. J. Zheng, F. Qi, J. R. He and B. Yu, *Mater. Lett.*, 2017, **197**, 67.

43 M. K. Chen, Y. F. Wang, N. Shepherd, C. Huard, J. T. Zhou, L. J. Guo, W. Lu and X. G. Liang, *ACS Nano*, 2017, **11**, 1091.

44 Eftekhari, *J. Mater. Chem. A*, 2017, . DOI: 10.1039/C7TA04268J

45 A. H. Loo, A. Bonanni, Z. Sofer and M. Pumera, *Electrochem. Comm.*, 2015, **50**, 39.

46 Z. Liu, H. Zhao, N. Li, Y. Zhang, X. Zhang and Y. Du, *Inorg. Chem. Front.*, 2016,

View Article Online
DOI: 10.1039/C7AN01244F

3, 313.

47 W. Li, D. H. Chen, F. Xia, J. Z. Y. Tan, J. C. Song, W. G. Song and R. A. Caruso, *Chem. Commun.*, 2016, **52**, 4481.

48 Y. N. Wu, J. Huang, X. H. Yang, Y. J. Yang, K. Quan, N. L. Xie, J. Li, C. B. Ma, and K. M. Wang, *Anal. Chem.*, 2017, DOI: 10.1021/acs.analchem.7b01632

49 D. D. Zeng, Z. H. Wang, Z. Q. Meng, P. Wang, L. L. San, W. Wang, A. Aldalbahi, L. Li, J. W. Shen and X. Q. Mi, *ACS Appl. Mater. Interfaces*, 2017, **9**, 24118.

50 H. T. Xiong and X. W. Zheng, *Microchim. Acta*, 2017, **184**, 1781.

51 Q. Li, Q. Wang, X. H. Yang, K. M. Wang, H. Zhang and W. Y. Nie, *Talanta*, 2017, **174**, 521.

52 L. Tian, K. Qian, J. X. Qi, Q. Y. Liu, C. Yao, W. Song, Y. H. Wang, *Biosens. Bioelectron.*, 2018, **99**, 564.

53 Shao Su , Wenfang Cao, Wei Liu, Zaiwei Lu, Dan Zhu, Jie Chao, Lixing Weng, Lihua Wang, Chunhai Fana, Lianhui Wang, *Biosens. Bioelectron.*, 2017, **94**, 552.

View Article Online
DOI: 10.1039/C7AN01244F

Supporting Information

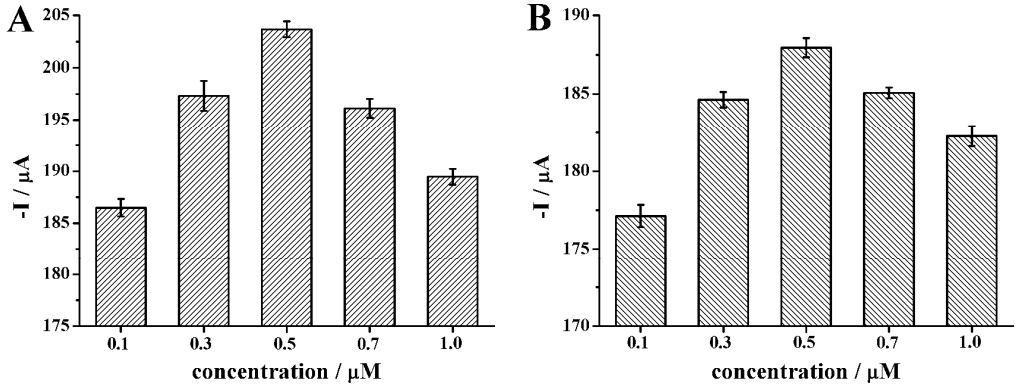

Fig. S1. The influence of concentration of SH-RNA (A) and streptavidin-HRP (B) on peak current.